

Dirac cones and chiral selection of elastic waves in a soft strip

Maxime Lanoy^{a,1}, Fabrice Lemoult^a, Antonin Eddi^b, and Claire Prada^a

^aInstitut Langevin, ESPCI Paris, PSL University, CNRS, 75005 Paris, France; ^bPMMH, CNRS, ESPCI Paris, Université PSL, Sorbonne Université, Université de Paris, F-75005, Paris, France

This manuscript was compiled on March 17, 2024

We study the propagation of in-plane elastic waves in a soft thin strip; a specific geometrical and mechanical hybrid framework which we expect to exhibit Dirac-like cone. We separate the low frequencies guided modes (typically 100 Hz for a centimetre wide strip) and obtain experimentally the full dispersion diagram. Dirac cones are evidenced together with other remarkable wave phenomena such as negative wave velocity or pseudo-zero group velocity (ZGV). Our measurements are convincingly supported by a model (and numerical simulation) for both Neumann and Dirichlet boundary conditions. Finally, we perform one-way chiral selection by carefully setting the source position and polarization. Therefore, we show that soft materials support atypical wave-based phenomena, which is all the more interesting as they make most of the biological tissues.

Dirac cone | Soft matter | Elastic waves | Chiral waves

Graphene has probably become the most studied material in the last decades. It displays unique electronic properties resulting from the existence of the so-called Dirac cones (1). At these degeneracy points, the motion of electrons is described in quantum mechanics by the Dirac equation: the dispersion relation becomes linear and electrons behave like massless fermions (2). As a result, interesting transport phenomena such as the Klein tunneling or the *Zitterbewegung* effect have been reported (3). But Dirac cones are not specific to graphene. They correspond to transition points between different topological phases of matter (4). This discovery has enabled the understanding of topologically protected transport phenomena, such as the quantum Hall effect (5). Dirac cones are the consequence of a specific spatial patterning rather than a purely quantum phenomenon. Inspired by these tremendous findings from condensed matter physics, the wave community thus started to search for classical analogs in photonic crystals (6, 7). Abnormal transport properties similar to the *Zitterbewegung* effect were highlighted (8, 9). In recent years, the quest for photonic (and phononic) topological insulators (10) has become a leading topic. This specific state of matter results from the opening of a band gap at the Dirac frequency and is praised for its application to robust one-way wave-guiding (11, 12). Surprisingly, similar degeneracies have been observed for unexpected photonic lattices as the consequence of an accidental adequate combination of parameters (13). Such Dirac-like cones have a fundamentally different nature as they occur in the $k \rightarrow 0$ limit (14) but still offer interesting features: wave-packets propagate with a non-zero group velocity while exhibiting no phase variation, just like in a zero-index material (15, 16).

A similar accidental $k \rightarrow 0$ Dirac-like cone can be observed in the dispersion relation of elastic waves propagating in a simple plate. In this context, the cone results from the coincidence of two cut-off frequencies occurring when the

Poisson's ratio is exactly of $\nu = 1/3$ (17–20). This condition seriously restricts the amount of potential materials to nearly the Duraluminum or zircalloy. However, a recent investigation emphasized that the in-plane modes of a thin strip are analogous to Lamb waves propagating in a plate of Poisson's ratio $\nu' = \nu/(1+\nu)$ (21). The degeneracy should then occur in the case of incompressible materials ($\nu = 1/2$). This indicates that the strip configuration is the perfect candidate for the observation of Dirac cones in the world of soft matter. Due to their nearly-incompressible nature, soft materials indeed present interesting dynamical properties embodied by the propagation of elastic waves: the velocity of the transversely polarized waves is several orders of magnitudes smaller than its longitudinal counterpart. This aspect has been at the center of interesting developments in various contexts from evidencing the role of surface tension in soft solids (22, 23) to model experiments for fracture dynamics (24) or transient elastography (25, 26).

In this article, we study in-plane elastic waves propagating in a soft (*i.e.* incompressible and highly deformable) thin strip and propose an experimental platform to monitor the propagation of the in-plane displacement thanks to a particle tracking algorithm. We provide full experimental and analytical description of these in-plane waves both for free and rigid edge conditions. We notably extract the low-frequency part of the dispersion diagram for the two configurations. We clearly evidence the existence of Dirac-like cones for this simple geometry and highlight some other remarkable wave phenomena such as backward modes or zero group

Significance Statement

Thanks to particle tracking methods, we monitor the propagation of in-plane elastic waves in an incompressible thin strip and observe, for the first time, a Dirac cone in a soft material. Additional remarkable wave features such as negative phase velocities, pseudo zero group velocity and one-way chiral selection are highlighted. Our findings are universal: any thin strip made of any soft elastomer will display the same behavior. Dirac cones have inspired many developments in the condensed matter field over the last decade. Our findings enable the search for analogues in the realm of soft matter, leading to a wide range of potential applications. Additionally, they are of practical interest for biologists since soft strips are ubiquitous among human tissues and organs.

All authors participated in the conception of the project, the setting up of the experiment, the data processing and in writing down the article. F.L. and M.L. ran the numerical simulations. C.P. provided the theoretical description. A.E. provided the rheological measurements.

¹To whom correspondence should be addressed. E-mail: maxime.lanoy@gmail.com

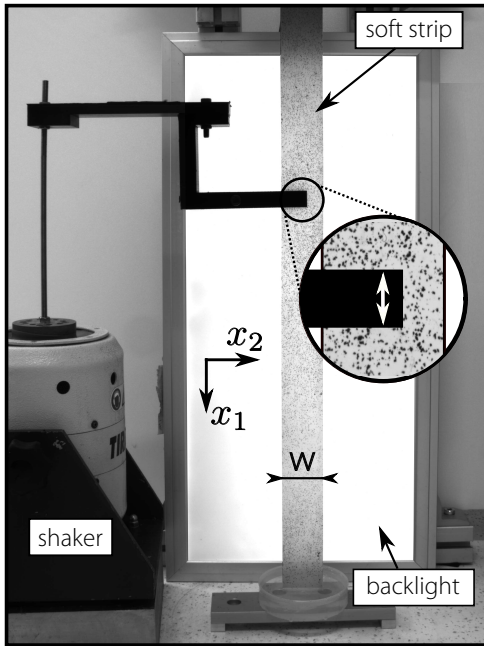


Fig. 1. Experimental setup: a soft elastic strip (of dimensions $L = 600$ mm, $w = 39$ mm, $d = 3$ mm) seeded with dark pigments (for motion tracking purposes) is suspended. A shaker connected to a clamp induces in-plane displacement propagating along the strip.

velocity (ZGV) modes. Eventually, we perform chiral selective excitation resulting in the propagation of one-way state, and in the separation of the two contributions of a ZGV wave.

Experimental configuration. To start off, a thin strip of dimensions $L \times w \times d = 600$ mm \times 39 mm \times 3 mm is prepared in a soft silicone elastomer (for details see section Materials and Methods) and seeded with dark pigments for tracking purposes. The strip is then suspended and connected to a point-like source consisting of a clamp mounted on a low-frequency (1 Hz to 200 Hz) shaker. When vibrated, the strip hosts the propagation of guided elastic waves travelling along the vertical direction x_1 (see Fig. 1). The lower end of the strip is immersed in glycerol to avoid spurious reflections as well as out-of plane motions. Here, we specifically study in-plane motions *i.e.* displacement components u_1 and u_2 corresponding to respective directions x_1 and x_2 . The low-frequency regime enables the optical monitoring of the in plane motion. A 60 images sequence corresponding to a single wave period is acquired thanks to stroboscopic means before being processed with a Digital Image Correlation (DIC) algorithm (27) which retrieves the displacement of the dark seeds. Typical displacement fields (u_1 , u_2) measured when shaking at 110 Hz are reported on Fig. 2(a). This method is sensitive to displacement magnitudes in the micrometer range and thus enables field extraction to be performed over large areas in spite of the significant viscous damping.

Free edges configuration. The interpretation of the displacement maps is not straightforward. As for any wave-guiding process the field gathers contributions from several modes. Given the system geometry, we project the data on their sym-

metrical (resp. anti-symmetrical) component with respect to the vertical central axis. For improved extraction performances, a single value decomposition (SVD) is then operated and only the significant solutions are kept (for details see the Supporting Information). For example, at 110 Hz, the raw data (see Fig. 2) gathers three main contributions: two anti-symmetrical modes (denoted A_0 and A_1) and one symmetrical mode (S_0). Each mode goes along with a single spatial frequency k which we extract by Fourier-transforming the right-singular vectors (containing the information relative to the x_1 direction). Repeating this procedure for frequencies ranging from 1 to 200 Hz, one obtains the full dispersion diagram displayed in Fig. 2(c) (filled symbols correspond to values directly extracted from the data, while empty ones are obtained by symmetry with respect to the $k = 0$ axis). The dispersion diagram reveals several branches with different symmetries and behaviors. Here, the branches are indexed with increasing cut-off frequencies. Note that, due to viscous dissipation, the wave-number k is intrinsically complex valued. As a matter of fact, this is well pictured by the decaying character of the field maps (Fig 2). The Fourier analysis yields its real part (peaks location) but also its imaginary part (peaks width) which is provided in Fig. S4 (Supporting Information).

Those experimental results are in good agreement with theoretical predictions (solid line) obtained with a simplified model and by numerical simulation (both are presented in Supporting Information). Indeed, one can show that the in-plane modes of a given strip are analogous to the Lamb waves propagating in a virtual 2-D plate of appropriate effective mechanical properties (21). When the strip is made of a soft material, the analogy holds for a plate of thickness w , with a shear wave velocity of v_T , a longitudinal velocity of exactly $2v_T$. Strikingly, this amounts to acknowledging that, for a thin strip of soft material, the low frequency in-plane guided waves are independent of the bulk modulus (or equivalently of the longitudinal wave velocity) and of the strip thickness d . One can then retrieve the full dispersion solely from the knowledge of the strip's shear modulus G , width w and density ρ . Of course, the intrinsic dispersive properties of the soft material as well as its lossy character must be taken into account. A simple and commonly accepted model for describing the low frequency rheology of silicone polymers is the fractional Kelvin-Voigt model (28–30), for which the complex shear modulus writes $G = G_0 [1 + (i\omega\tau)^n]$. This formalism being injected in the 2-D model, our measurements are convincingly adjusted (solid lines in Fig. 2) when the following set of parameters is input: $G_0 = 26$ kPa, $\tau = 260$ μ s and $n = 0.33$. Note that this choice of parameters turns out to match relatively well the measurements obtained with a traditional rheometer (see details in Supporting Information). The transparency of the theoretical line represents the weight of the imaginary part of the wave-number k (detailed on Fig. S5). When k becomes essentially imaginary, the solution is evanescent which explains why it cannot be extracted from the experiment.

Let us now comment on a few interesting features of this dispersion diagram. First, at low frequencies, the single symmetrical branch (labelled S_0) presents a linear slope, hence defining a non-dispersive propagation or equivalently a propagation at constant wave velocity. Experimentally, the latter corresponds to $\sqrt{3}v_T$ which confirms the prediction from (21). This is somehow counter-intuitive: the displacement of S_0 is

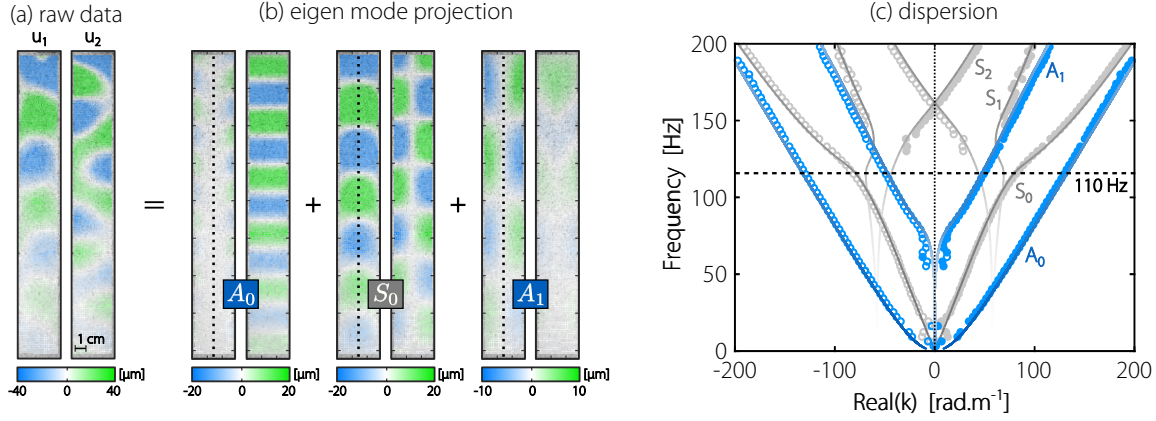


Fig. 2. Free edges field maps and dispersion. Here $w = 39$ mm. (a) Real part of the raw displacements at 110 Hz and (b) the three corresponding singular vectors (see text). (c) Experimental (symbols) and analytical (solid lines) dispersion curves. Transparency renders the ratio $\text{Im}(k)/\text{Abs}(k)$ (see Supplementary Information). Filled gray and blue symbols correspond to extracted symmetrical and anti-symmetrical modes. Empty ones are obtained by symmetry.

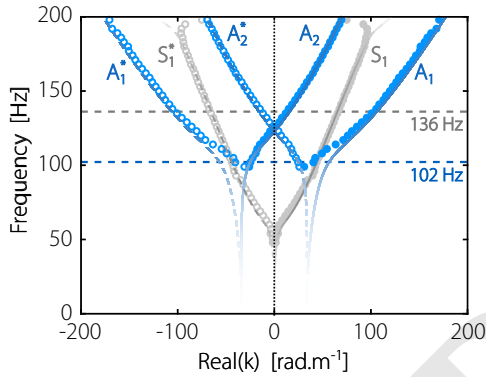


Fig. 3. Fixed edges dispersion. Experimental (symbols) and theoretical (solid lines) dispersion curves for a strip of width $w = 50.6$ mm with fixed edges. Symmetrical modes (resp. anti-symmetrical) are labelled in gray (resp. blue). Similarly to Fig. 2c, the transparency renders the ratio $\text{Im}(k)/\text{Abs}(k)$ (see Supplementary Information). Filled gray and blue symbols correspond to extracted symmetrical and anti-symmetrical modes. Empty ones are obtained by symmetry.

quasi-exclusively polarized along the x_1 direction, giving it the aspect of a pseudo-longitudinal wave, but it propagates at a speed independent of the longitudinal velocity. At 150 Hz, two branches cross linearly in the $k \rightarrow 0$ limit. This is the signature of a Dirac-like cone (13, 18, 31). It is worth mentioning that, despite the 3-D character of the system, the propagation only occurs in one direction (x_1) which means that the cone should be regarded as a linear crossing. Its slope (group velocity) is found to be $\pm 2v_T/\pi$ (see calculation in Supporting Information). The cone, which turns out to be well defined in spite of the significant damping, directly results from the incompressible nature of the soft elastomer. Indeed, the condition $v_L \gg v_T$ (*i.e.* $\nu \approx 1/2$) automatically yields the coincidence of the second and third cut-off frequencies (21). In other words, any thin soft strip would display such a Dirac-like cone. Because the cone is located at $k = 0$, the lower frequency part of the S_2 branch features negative wave numbers (solid symbols). In this region, the phase and group velocities are anti-parallel (32, 33). More specifically, the group velocity remains positive (as imposed by causality) when the phase

velocity becomes negative *i.e.* the wave-fronts travel toward the source (see video S3). This effect has been the scope of many developments in the metamaterials field (34, 35) but occurs spontaneously here.

Fixed edges configuration. From now on, we implement Dirichlet boundary conditions on a $w = 50.6$ mm strip by clamping its edges in a stiff aluminium frame (video S4). Again, the dispersion curves (Fig. 3) are extracted following the previous experimental steps. See how the low order branches (A_0 and S_0 in Fig. 2(b)) have disappeared as a consequence of the field cancellation at the boundaries. Besides, a Dirac-like cone is observed for this configuration as well but it now occurs at the crossing of anti-symmetrical branches. Just like in the free edges configuration, the slope at the Dirac point is $v_g = \pm 2v_T/\pi$. Extracting the field patterns for this particular point, one finds that the motion is elliptical (video S5). The polarization even becomes circular at a distance $\pm w/6$ from the centre of the strip. All these observations are supported by the calculation provided in Supporting Information.

Once again, the prediction obtained with the 2-D equivalence model assuming rigid boundaries convincingly matches the experiment. Also, an interesting feature shows up at 102 Hz where the branches A_1 and A_2^* nearly meet each-other. In a non-dissipative system, one expects the two branches to connect thus yielding a singular point associated with a Zero Group Velocity (ZGV); a phenomenon which has been previously observed in rigid plates (36–40). Here, because the propagation is damped by viscous mechanisms, the connection does not strictly occur, the reason why we talk about pseudo-ZGV mode, but as we will see below similar wave phenomena still exist in the presence of damping (see Fig. S2 for an analytical comparison between the conservative and dissipative scenarii).

Let us now illustrate the rich physics associated to this dispersion diagram by specifically selecting a few interesting modes (videos S6 to S9). To begin with, the source is placed in the centered and shaken vertically at 136 Hz. This excitation is intrinsically symmetrical and only S_1 should be fed at this frequency. The chronophotographic sequence displayed on

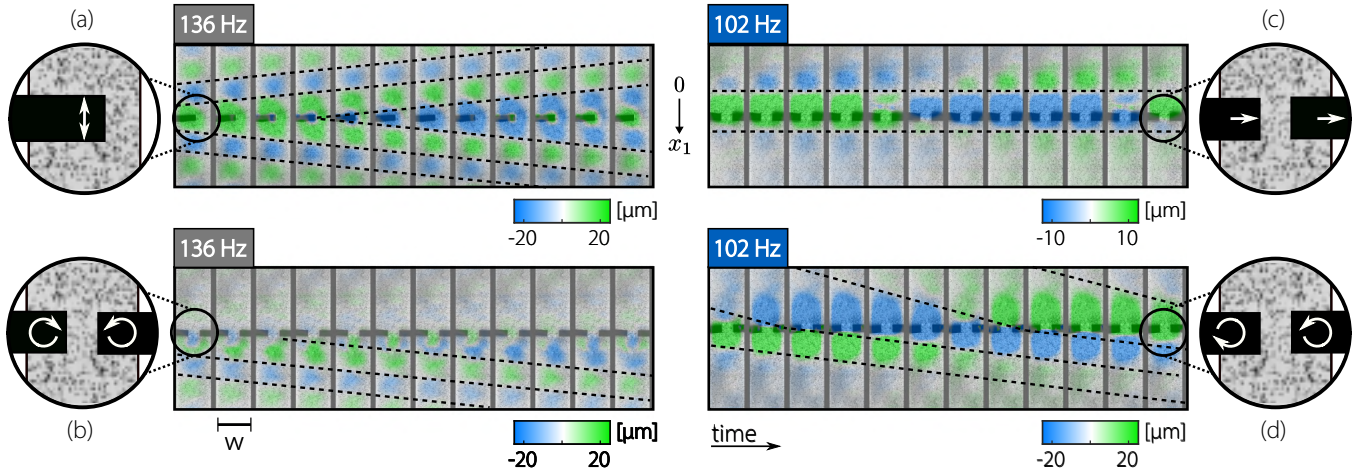


Fig. 4. Selective generation. Chronophotographic sequences (12 snapshots) over a full oscillation cycle. (a) The source is placed at the centre of the strip and shaken vertically at 136 Hz: symmetric diverging waves are observed on both parts. (b) Two sources facing each other are rotated in opposite directions at 136 Hz: the wave only travels to the $x_1 > 0$ region. (c) Two sources are shaken horizontally at 102 Hz: a stationary wave associated to an anti-symmetric pseudo-ZGV mode is observed. (d) The two sources are rotated at 102 Hz in an anti-symmetrical manner: The propagation is restored and the phase velocity is negative in the on the top region ($x_1 < 0$). The black dashed lines are visual guides highlighting the zeroes of displacement and the sketches show the source shape and motion. For sake of clarity, one only represents u_1 for (a) and (b) and u_2 for (c) and (d). See videos S6 to S9 in supporting information for more details.

Fig. 4(a) reports twelve successive snapshots of the displacement u_1 taken over a full period of vibration at 136 Hz. As expected, the field pattern respects the S_1 symmetry. Also, the zeroes of the field (red dashed lines) move away from the source, which corresponds to diverging waves.

On either side of the strip, there are two solutions with identical profiles but opposite phase velocities; in other words two time-reversed partners. Thus, the bottom part of the strip hosts the solution S_1 while its top part supports S_1^* . Furthermore, the transverse field u_2 is $\pi/2$ phase shifted compared to u_1 at this frequency (see Fig. S7 or video S6). This essentially suggests that the in-plane displacement is elliptically polarized; an interesting feature since such a polarization is known to flip under a time-reversal operation. One can easily take advantage of this effect by imposing a chiral excitation. To this end, we use a source made of two counter-rotating clamps located at equal distances from the centre of the strip. The rotating motion is produced by driving two distinct clamps with 4 different speakers connected to a soundboard (Presonus AudioBox 44VSL). As depicted in Fig. 4(b), such a chiral source excites the S_1 mode which propagates towards $x_1 > 0$, however, it cannot produce its time reverse partner S_1^* propagating in the opposite direction. By controlling the source's chirality, we performed selective feeding and one-way wave transport, a feature which has recently been exploited in different contexts (41–43).

One can also try to capture the strip behaviour near the pseudo ZGV point. As it is associated with an anti-symmetrical motion, the system is shaken horizontally by two clamps driven simultaneously at 102 Hz, and the field displacement u_2 over a full cycle is represented in Fig. 4(c). It exhibits a very unique property: the zeroes remain still (see dashed lines) whatever the phase within the cycle which indicates that the solution is stationary. To understand this feature, let us take a look back at Fig. 3. Causality imposes that A_1 and A_2 (filled symbols, solid lines) propagate in the bottom part of

the strip while their time partners A_1^* and A_2^* (empty symbols, dashed lines) travel toward the top part. Interestingly, at 102 Hz, A_1 and A_2 (resp. A_1^* and A_2^*) have almost opposite wave numbers and interfere to produce a standing wave. The stationarity does not result from some reflection at the strip ends but is a direct consequence of the coincidence of the two branches. In our damped case where the exact coincidence seems lost, the difference in magnitudes between the respective wavenumbers is sufficiently small to guarantee this effect at the pseudo-ZGV frequency.

Again, introducing some chirality will result in breaking the time-reversal symmetry. The sources are now rotated in an anti-symmetrical manner (see inset) resulting in the measurements reported on Fig. 4(d). The propagative nature of the field is retrieved on both sides: the zeroes of the field are travelling. Note that, on the upper part, the wave-fronts are anti-causal, *i.e.* they seem to move towards the source which is typical of a negative phase velocity. Strictly speaking, only A_1 (resp A_2^*) remains in the lower part (resp. upper part) of the strip. Thanks to the chiral excitation, we have separated the two contributions of a pseudo-ZGV point, and highlight their unique nature as a superposition of two modes propagating in opposite directions.

Perspectives. In this article, we report the observation of Dirac-like cones in a soft material in spite of a significant dissipation due to viscous effects. The associated dispersion is also found to induce atypical wave phenomena such as a negative phase velocity and a stationary mode. For both the Dirichlet and Neumann boundaries, a convincing agreement is found between experiments, the theoretical simplified model and numerical analysis. Additionally, we perform selective feeding by controlling the chirality of the source. Beyond the original wave physics, the soft strip configuration may stimulate interest in different domains in a near future. From a material point of view, we show how a very simple platform

can provide comprehensive information about the visco-elastic properties of a soft solid leading to new technologies to probe its rheology. From a biological point of view, understanding the complex physics associated with a geometry that is ubiquitous in the human tissues and organs, is a major challenge. Imaging and therapeutic methods based on elastography would benefit from an in-depth understanding of the specific dynamic response of tendons (44), myocardium (45) or vocal cords (46) among others. Some physiological mechanisms could also be unveiled by accounting for the atypical vibrations of a soft strip. In the inner ear, for instance, the sound transduction is essentially driven by a combination of two soft strips namely the basilar and tectorial membranes (47–49). Overall, we might soon discover that evolution had long transposed the exceptional properties of graphene to the living world.

Materials and Methods

Sample preparation. The strips are prepared by molding a commercial elastomer (Smooth-On Ecoflex® 00-30). The monomer and cross-linking agent are mixed in a 1:1 ratio and left for curing for roughly half a day. Once cured, the measured polymer density is of $\rho = 1010 \text{ kg.m}^{-3}$. Rheological measurements are performed on a conventional apparatus (Anton-Paar MCR501) set in a plate-plate configuration. The results are available in Supporting Information.

Vibration. The strips are excited by a shaker (Tira Vib 51120) driven monochromatically with an external signal generator (Keysight 33220A) and amplifier (Tira Analog Amplifier BAA 500) with frequencies ranging from 1 to 200 Hz. A point-like excitation is ensured by connecting the shaker to a 3D-printed clamp tightening the strip at a specific location and designed with conical termination. Spurious out of plane vibrations are reduced by immersing the strip's bottom end in glycerol (visible in figure 1).

Motion tracking. During the curing stage, the blend is seeded with "Ivory black" dark pigments (the particles are smaller than $500 \mu\text{m}$) enabling to monitor the motion by Digital Image Correlation (DIC). Video imaging is performed with a wide-sensor camera (Basler acA4112-20um) positioned roughly 2 meters away from the strip (raw videos are available in Supporting Information). For each dataset, a 60-images sequence is acquired with an effective framerate set to 60 images per waveperiod (to capture exactly one wave oscillation). These relatively high effective framerates are reached by stroboscopy (the actual acquisition rate is larger than the waveperiod). The video data is then processed with the DIC algorithm (27) which renders 60×2 (u_1 and u_2) displacement maps for each frequency.

Post-processing. Retrieving the dispersion curves requires further processing. First, the monochromatic displacement maps are converted to a single complex map by computing a discrete time-domain Fourier transform. The data is then projected on its symmetrical and anti-symmetrical as a preliminary step to the SVD operation (details of the SVD are available in Supporting Information). After selecting the relevant singular vectors, the spatial frequencies are extracted by Fourier transformation.

ACKNOWLEDGMENTS. We thank Sander Wildeman for sharing his DIC algorithm, Gatién Clément for early experimental developments, Jérôme Laurent for sharing his Lamb modes dispersion code and Pascale Arnaud for video editing. This work has been supported by LABEX WIFI (Laboratory of Excellence within the French Program "Investments for the Future") under references ANR-10-LABX-24 and ANR-10-IDEX-0001-02 PSL*, and by Agence Nationale de la Recherche under reference ANR-16-CE31-0015.

1. AC Neto, F Guinea, NM Peres, KS Novoselov, AK Geim, The electronic properties of graphene. *Rev. modern physics* **81**, 109 (2009).
2. NW Ashcroft, ND Mermin, Solid state physics (saunders college, philadelphia, 1976). *Append. N* **166** (2010).
3. M Katsnelson, K Novoselov, A Geim, Chiral tunnelling and the klein paradox in graphene. *Nat. physics* **2**, 620–625 (2006).
4. MZ Hasan, CL Kane, Colloquium: topological insulators. *Rev. modern physics* **82**, 3045 (2010).

5. Kv Klitzing, G Dorda, M Pepper, New method for high-accuracy determination of the fine-structure constant based on quantized hall resistance. *Phys. Rev. Lett.* **45**, 494 (1980).
6. T Ochiai, M Onoda, Photonic analog of graphene model and its extension: Dirac cone, symmetry, and edge states. *Phys. Rev. B* **80**, 155103 (2009).
7. S Bittner, et al., Observation of a dirac point in microwave experiments with a photonic crystal modelling graphene. *Phys. Rev. B* **82**, 014301 (2010).
8. RA Sepkhanov, YB Bazaliy, CWJ Beenakker, Extremal transmission at the dirac point of a photonic band structure. *Phys. Rev. A* **75**, 063813 (2007).
9. X Zhang, Z Liu, Extremal transmission and beating effect of acoustic waves in two-dimensional sonic crystals. *Phys. Rev. Lett.* **101**, 264303 (2008).
10. T Ozawa, et al., Topological photonics. *Rev. Mod. Phys.* **91**, 015006 (2019).
11. AB Khanikaev, et al., Photonic topological insulators. *Nat. materials* **12**, 233–239 (2013).
12. LH Wu, X Hu, Scheme for achieving a topological photonic crystal by using dielectric material. *Phys. review letters* **114**, 223901 (2015).
13. X Huang, Y Lai, ZH Hang, H Zheng, C Chan, Dirac cones induced by accidental degeneracy in photonic crystals and zero-refractive-index materials. *Nat. materials* **10**, 582–586 (2011).
14. J Mei, Y Wu, CT Chan, ZQ Zhang, First-principles study of dirac and dirac-like cones in phononic and photonic crystals. *Phys. Rev. B* **86**, 035141 (2012).
15. F Liu, X Huang, C Chan, Dirac cones at $k \rightarrow 0$ in acoustic crystals and zero refractive index acoustic materials. *Appl. Phys. Lett.* **100**, 071911 (2012).
16. P Moitra, et al., Realization of an all-dielectric zero-index optical metamaterial. *Nat. Photonics* **7**, 791–795 (2013).
17. RD Mindlin, *An introduction to the mathematical theory of vibrations of elastic plates*. (Singapore: World Scientific, Ed. J. Yang), pp. 23–78 (2006).
18. A Maznev, Dirac cone dispersion of acoustic waves in plates without phononic crystals. *The J. Acoust. Soc. Am.* **135**, 577–580 (2014).
19. DM Stobbe, TW Murray, Conical dispersion of lamb waves in elastic plates. *Phys. Rev. B* **96**, 144101 (2017).
20. DM Stobbe, CM Grunsteidl, TW Murray, propagation and scattering of lamb waves at conical points in plates. *Sci. reports* **9**, 1–10 (2019).
21. J Laurent, D Royer, C Prada, In-plane backward and zero-group-velocity guided modes in rigid and soft strips. *The J. Acoust. Soc. Am.* **147** (2020).
22. X Shao, J Saylor, J Bostwick, Extracting the surface tension of soft gels from elastocapillary wave behavior. *Soft matter* **14**, 7347–7353 (2018).
23. P Chantelot, L Domino, A Eddi, How capillarity affects the propagation of elastic waves in soft gels. *Phys. Rev. E* **101**, 032609 (2020).
24. A Livne, G Cohen, J Fineberg, Universality and hysteretic dynamics in rapid fracture. *Phys. review letters* **94**, 224301 (2005).
25. L Sandrin, M Tanter, JL Gennisson, S Catheline, M Fink, Shear elasticity probe for soft tissues with 1-d transient elastography. *IEEE transactions on ultrasonics, ferroelectrics, frequency control* **49**, 436–446 (2002).
26. J Bercoff, M Tanter, M Fink, Supersonic shear imaging: a new technique for soft tissue elasticity mapping. *IEEE Transactions on Ultrason. Ferroelectr. Freq. Control.* **51**, 396–409 (2004).
27. S Wildeman, Real-time quantitative schlieren imaging by fast fourier demodulation of a checked backprop. *Exp. Fluids* **59**, 97 (2018).
28. FC Meral, TJ Royston, RL Magin, Surface response of a fractional order viscoelastic half-space to surface and subsurface sources. *The J. Acoust. Soc. Am.* **126**, 3278–3285 (2009).
29. SP Kearney, A Khan, Z Dai, TJ Royston, Dynamic viscoelastic models of human skin using optical elastography. *Phys. Medicine & Biol.* **60**, 6975 (2015).
30. E Rolley, JH Snoeijer, B Andreotti, A flexible rheometer design to measure the visco-elastic response of soft solids over a wide range of frequency. *Rev. scientific instruments* **90**, 023906 (2019).
31. DM Stobbe, TW Murray, Conical dispersion of lamb waves in elastic plates. *Phys. Rev. B* **96**, 144101 (2017).
32. S Brahamavar, et al., Negative refraction and focusing of elastic lamb waves at an interface. *Phys. Rev. B* **83**, 014106 (2011).
33. FD Philippe, TW Murray, C Prada, Focusing on plates: controlling guided waves using negative refraction. *Sci. reports* **5**, 11112 (2015).
34. PA Deymier, *Acoustic metamaterials and phononic crystals*. (Springer Science & Business Media) Vol. 173, (2013).
35. R Craster, S Guenneau, *World Scientific Handbook of Metamaterials and Plasmonics*. (World Scientific), (2017).
36. SD Holland, DE Chimenti, Air-coupled acoustic imaging with zero-group-velocity lamb modes. *Appl. physics letters* **83**, 2704–2706 (2003).
37. C Prada, O Balogun, T Murray, Laser-based ultrasonic generation and detection of zero-group velocity lamb waves in thin plates. *Appl. Phys. Lett.* **87**, 194109 (2005).
38. C Prada, D Clorennec, D Royer, Local vibration of an elastic plate and zero-group velocity lamb modes. *The J. Acoust. Soc. Am.* **124**, 203–212 (2008).
39. C Prada, D Clorennec, D Royer, Power law decay of zero group velocity Lamb modes. *Wave Motion* **45**, 723–728 (2008).
40. C Grunsteidl, TW Murray, T Berer, IA Veres, Inverse characterization of plates using zero group velocity Lamb modes. *Ultrasonics* **65**, 1–4 (2016).
41. C Shi, et al., Observation of acoustic spin. *Natl. Sci. Rev.* **6**, 707–712 (2019).
42. Y Long, et al., Symmetry selective directionality in near-field acoustics. *Natl. Sci. Rev.* **7**, 1024–1035 (2020).
43. S Yves, G Leroisey, F Lemout, Structure-composition correspondence in crystalline metamaterials for acoustic valley-Hall effect and unidirectional sound guiding. *EPL (Europhysics Lett.)* **129**, 44001 (2020) Publisher: IOP Publishing.
44. J Brum, M Bernal, J Gennisson, M Tanter, In vivo evaluation of the elastic anisotropy of the human achilles tendon using shear wave dispersion analysis. *Phys. Medicine & Biol.* **59**, 505 (2014).
45. IZ Nenadic, MW Urban, SA Mitchell, JF Greenleaf, Lamb wave dispersion ultrasound vibrometry (Iduv) method for quantifying mechanical properties of viscoelastic solids. *Phys. Medicine*

- & *Biol.* **56**, 2245 (2011).
46. K Ishizaka, N Isshiki, Computer simulation of pathological vocal-cord vibration. *The J. Acoust. Soc. Am.* **60**, 1193–1198 (1976).
 47. T Reichenbach, A Hudspeth, The physics of hearing: fluid mechanics and the active process of the inner ear. *Reports on Prog. Phys.* **77**, 076601 (2014).
 48. JB Sellon, S Farrahi, R Ghaffari, DM Freeman, Longitudinal spread of mechanical excitation through tectorial membrane traveling waves. *Proc. Natl. Acad. Sci.* **112**, 12968–12973 (2015).
 49. JB Sellon, et al., Nanoscale poroelasticity of the tectorial membrane determines hair bundle deflections. *Phys. Rev. Lett.* **122**, 028101 (2019).

DRAFT